

## Effect of Inlet Air Pre-Cooling of Water Injection on Compressor Performance at High Flight Mach

A. Q. Lin, Q. Zheng, L. Yang and H. Zhang<sup>†</sup>

*College of Power and Energy Engineering, Harbin Engineering University, Harbin 150001, Heilongjiang Province, China*

<sup>†</sup>Corresponding Author Email: zanghai83821@163.com

(Received May 19, 2018; accepted September 3, 2018)

### ABSTRACT

In high altitude and Mach number, the inflow air with the high temperature will influence on the aero-engine performance while the mass injection pre-compressor cooling (MIPCC) technology is one of the problem-solving ways to reduce high temperature. To explore the convection coupling process between droplet and inflow air, the compressible Reynolds average N-S equations in the compressor coupled with the pre-cooling section is solved by the finite volume method to analyze its performance changes at different water injection rates and droplet sizes. Results show that, in the flight of 3.5 Mach number, the larger water injection rate easily form the shock wave due to the disturbance of droplets in the pre-cooling section. Furthermore, the temperature on the pressure surface near the trailing edge of the rotor blade aggravates along the radial migration, leading to uneven temperature distribution in the radial direction. Within the water injection rates of 0-8% and the particle sizes of 10-20  $\mu\text{m}$ , the inflow mass flow of air improves by 15.3-31.4%; the temperature ratio of compressor drops by 3.6-16.14%, which results in the decrease of specific compression work of the compressor and the changing trend from “increasing” to “decreasing” for the compressor efficiency.

**Keywords:** Compressor performance; High Mach; Water injection; MIPCC; Pre-cooling section.

### NOMENCLATURE

$A$	surface area of the rotor blade	$r$	radius of the rotor blade
$C_p$	specific heat	$T_t$	total temperature
$d$	droplet diameter	$P_t$	total pressure
$\bar{d}$	mean droplet diameter	$W_{\text{injection}}$	actual consumption power with the MIPCC method
$f_{\text{H}_2\text{O}}$	mass fractions of water vapor	$W_{\text{non-injection}}$	actual consumption power without the MIPCC method
$G$	mass flow		
$\bar{G}$	equivalent mass flow		
$L$	rotor blade torque		
MIPCC	mass injection pre-compression cooling	$\kappa$	ratio of specific heat capacity
$n$	distribution parameter	$\lambda$	thermal conductivity
$R_g$	gas constant of air	$\mu$	dynamic viscosity
$R_p$	total pressure ratio	$\phi$	physical properties
$R$	cumulative mass fraction	$\omega$	angular velocity

### 1. INTRODUCTION

When the aeroengine works at the conditions of high altitude and high speed, the kinetic energy of the incoming flow is irreversible to convert to the heat energy as a result of high-speed air flow compression, so that the temperature in front of

compressor increases to affect the engine performance. However, the pre-cooling technology can reduce the air temperature, increase the intake mass flow, effectively extend the high Mach number range and increase the thrust of aeroengine (Zou *et al.* 2015; Wang *et al.* 2016; Rui *et al.* 2015). In view of this, it is worth exploring a method of

pre-cooling in the engine.

Pre-cooling technology, that is, before the compressor to add the pre-cooling device, to solve the problem of high temperature flow at high-Mach flight. At present, some countries have also proposed solutions and a large number of experimental studies. The first solution is the fuel pre-cooling program, which is the cryogenic air turbine engine (ATRDC) developed in Russia (Vladimir 2007). ATRDC uses the pre-cooler to add the fuel liquid hydrogen to realize deeply cool the flow, so that temperature reduces to the liquefaction point above. Japan proposes the Air Turbo Ramjet Engine with eXpander cycle (ATREX) (Miyagi *et al.* 1995; Tanatsugu *et al.* 1997), through the installation of a jet device sprayed liquid nitrogen to the flow channel to prevent the icing problem on the prep-cooler surface. The second solution is the supercritical pre-cooling program, that is, the United Kingdom proposes the pre-cooling combined cycle engine (SABRE) (Steelant *et al.* 2011), this kind of strong pre-cooling heat exchanger with a smaller flow loss to get a greater heat transfer, the usage of supercritical state heat exchanger with micro-scale heat transfer unit to achieve cooling effect, to achieve a compact fast heat transfer. The above two schemes are based on the principle of the pre-cooler, avoiding the phase transition process and the energy conversion of latent heat of phase change. However, MIPCC-TBCC (Carter *et al.* 2003), which is a mass injection pre-compression cooling scheme (MIPCC) proposed by the United States, sets up one liquid-injection and two water-injection devices, requiring that the amount of water-injection does not exceed the volume of water saturation and liquid oxygen content is maintained at 20.9% of the air flow. Balepin *et al.* (2001), Preston (2002) and Mehta *et al.* (2015) investigated the MIPCC technology for the theoretical research and verification, and they found that water injection technology performed faster and promoted the engine to enhance performance and broaden the flight envelope. As the saturated wet air moisture content increases with the increasing of temperature, when pressure is an atmospheric pressure, the saturated wet air at the temperature of 350K has more than the moisture content of 0.5, and injection pre-cooling conditions under the high temperature, the flow is very difficult to exceed moisture in the saturated air. However, too much water vapor mixed into the air will reduce the oxygen concentration of the working fluid leading to engine flameout (Balepin *et al.* 2003). Thus, David *et al.* (2005) through the F100 engine on the flight experiments utilizing the MIPCC method found that the water injection rate should not exceed 13% of the incoming mass flow at 3.5 Mach number. In summary, the mass injection technology has potential technical advantages and then has a certain significance and research value in the promotion of high Mach number power system.

Currently, the concept of water injection to cool down the air temperature by the application of the non-equilibrium evaporation phase transition and

heat transfer has also been tried before. White *et al.* (2010) and Neupert *et al.* (2014) studied the wet compression process for the droplets in the compressor. It was found that the heat action between the droplets and the air flow was a great influence on the flow field, and the droplets were more easily broken in a higher pneumatic load. Sun *et al.* (2012) numerically simulated the droplet motion in the wet compression process; they pointed out that droplets impinging on blades not only affected the movement and breakage of droplets but also caused additional loads on blades. White *et al.* (2004) discovered that the droplet diameter was the main factor of entropy increase in irreversible phase transformation. Moreover, Jiang *et al.* (2016) also proposed that mist droplet was a key factor affecting the heat transfer coefficient. For transient compressor characteristics in the process of droplet evaporation, the results from Kim *et al.* (2006) showed that the evaporation time of droplet was an important factor for the compressibility change. Then, the decrease of spray amount and droplet size were more conductive to the improvement of compressor performance. Sanaye *et al.* (2010) carried out that the water injection could effectively inhibit the temperature rise and improve the efficiency in the compressor. However, for inlet air pre-cooling of water injection, there is less research on compressor performance under the high-altitude Mach environment.

In this study, the transonic compressor of Stage-35, which is designed according to typical aeroengine requirements, is selected as the research object. And the pre-cooling technology in front of compressor, named as the pre-cooling section, is carried out. Based on the similarity theory which ensures the same equivalent mass flow, equivalent speed and Mach number to obtain the similarity flow field of high altitude flight conditions, the Euler-Lagrange multiphase flow model is used to investigate the non-equilibrium phase change cooling of droplet/air. The effect of inlet air cooling of water injection on aerodynamic performance is explored in the compressor coupled with the pre-cooling section.

## 2. NUMERICAL METHODOLOGY

### 2.1 Computation Model and Mesh

At present, there are two kinds of the MIPCC technology testing. First, high-altitude flight experiments (Preston *et al.* 2002; David *et al.* 2005); in order to meet the RASCAL project, MIPCC technology is applied to the F100 engine for high-altitude high Mach flight experiments, as shown in Fig. 1(a); Second, ground test (Balepin *et al.* 2003); applied to small turbofan engine simulation of high altitude condition to conduct on ground test for the mass injection pre-cooling, and the pre-cooling device shown in Fig. 1(b).

According to the MIPCC ground test scheme, the air cooling of water injection into the pre-cooling section will change the flow characteristic of

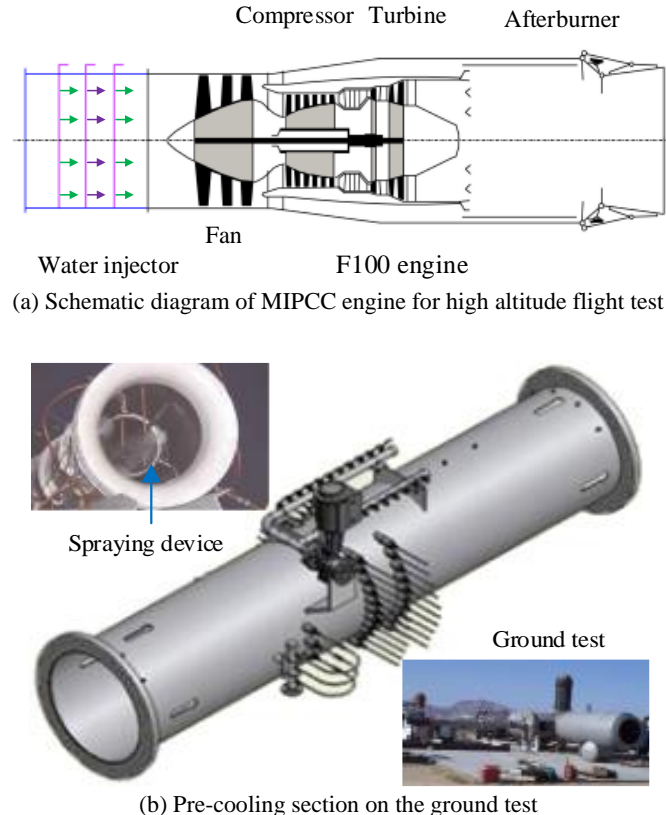


**Fig. 1. American MIPCC technology in high-altitude flight experiment and ground test.**

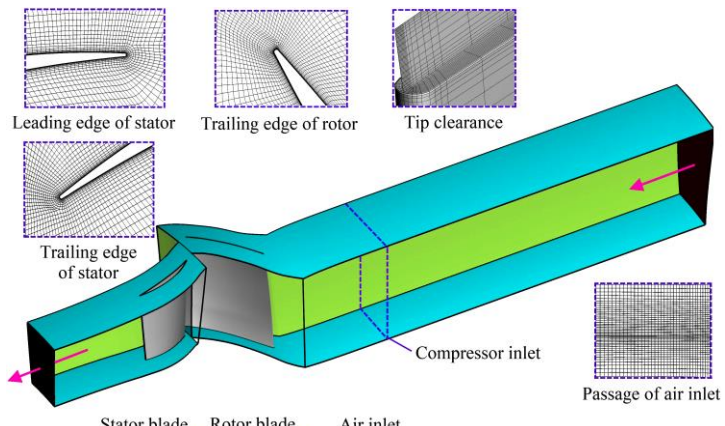


**Fig. 2. Stage-35 compressor computation domain and details of the leading edge, trailing edge and tip clearance mesh.**

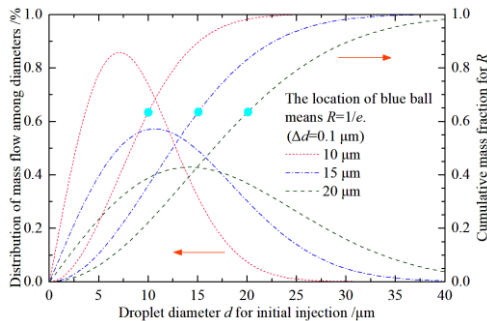
compressor at high altitude. So, it is necessary that the effect of MIPCC method on the aerodynamic performance is investigated. Table 1 gives the performance parameters of Stage-35 compressor at design point (Reid and Moore 1978).

The inlet domain, as the pre-cooling section in front of the compressor, is four times the chord length of the rotor blade so that the mass injection droplets are better mixed, flowed, evaporated and cooled with air. The computation domain and its mesh are shown in Fig. 2. The grid nodes are densely arranged in the region with the larger changing

gradient on pressure, velocity and temperature, and there are at least 18 nodes inside the boundary layer. The height of the first layer cell near wall is 5-10  $\mu\text{m}$ , and the density of global grid node distribution by natural transition. The Reynolds number is about  $2.17 \times 10^6$ , and Mach number of the incoming air is about 0.78. The averaged  $y^+$  value of all the walls is less than 2, which satisfies the requirement of the grid scale to the turbulence model. When the number of calculation grid is about 2.3 million, the sensitivity of grid numbers to the calculation results can be neglected.

**Table 1 Design performance parameters of Stage-35 compressor**

Parameters	Values	Parameters	Values
Rotation speed $N/(r/min)$	17188	Total temperature at inlet $T_t/K$	288.15
Mass flow $G/(kg/s)$	20.188	Total pressure at inlet $P_t/Pa$	101325
Tip speed /(m/s)	454.46	Efficiency/%	82.8

**Fig. 3. Initial mass fraction distribution of particle diameter for three mean droplet sizes.**

## 2.2 Numerical Model

The droplet particle is considered as the discrete phase owing to the volume fraction of the liquid is small, and the coming air is the continuous phase. The finite volume method is used to solve the governing equations of the continuous phase. The two-way coupling between the discrete phase and the continuous phase is realized through the source terms of the RANS equations. The Lagrangian method is used to track the droplet particles. Considering the influence of the particle transport models referring to Particle Wall Breakup model, Particle Collision model and Secondary Breakup model, the governing equations are closed by the low Reynolds number turbulence equations of SST  $\kappa-\omega$  model.

The droplets with the initial temperature of 288.15 K are ejected in the positive axial direction. Since the droplet hits the wall then produces the momentum loss, the normal and tangential rebound coefficients of droplet on the wall is set to 0.5. A liquid pressurized fan-shaped nozzle BIMV11002 (Ma 2013) is used for obtaining average droplet particle size of 10-50  $\mu m$  at a pressure of 0.1-0.3 MPa in order to evaporate the droplets as soon as possible. In this study, the mass flow rate of the mass injection in the pre-cooling section is 0-8% of the incoming flow; the mean droplet diameter  $\bar{d}$  (*i.e.*, the initial injected droplet size) is 10-20  $\mu m$  which conforms the Rosin-Rammler law (Lin et al. 2018) in present study. Then, the Rosin-Rammler particle distribution function is expressed by:

$$R = \exp[-(d/\bar{d})^n] \quad (1)$$

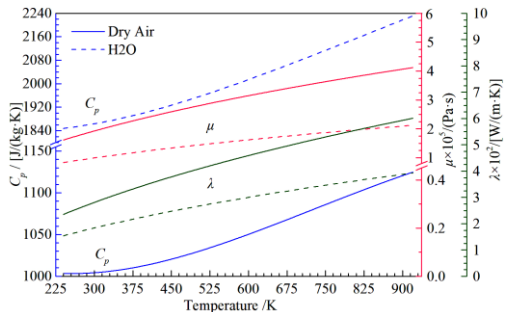
where,  $R$  is the cumulative mass fraction for those that are less than local droplet diameter  $d$ ,  $0 < R \leq 1$ ,  $\bar{d}$  is equal to the size at which  $R$  is  $1/e$ , and  $n$  is the

spread parameter. For the water problem, the typical range of values are of  $n = 1.5-3.0$ ; thus, this study is taken as 2.0 (Bayraktar and Yilmaz 2016).

To meet the effect of high temperature on physical properties of wet air mixture, the specific heat ( $C_p$ ) as a function of temperature is applied by a quartic polynomial, and the thermal conductivity ( $\lambda$ ) and dynamic viscosity ( $\mu$ ) of wet air mixture are taken from Sutherland's law. The properties of dry air and water vapor ( $H_2O$ ) are shown in Fig. 4. Thus, under different mass fractions of water vapor ( $f_{H2O}$ ) in the wet air, the weighted average property of wet air mixture ( $\Phi_{Mix}$ ) varying with temperature can be expressed as:

$$\Phi_{Mix} = \Phi_{H2O} \cdot f_{H2O} + \Phi_{Air} \cdot (1 - f_{H2O}) \quad (2)$$

where,  $\Phi$  represents  $C_p$ ,  $\mu$  and  $\lambda$ .

**Fig. 4. Physical properties of dry air and water vapor varying only with temperature.**

According to the American MIPCC scheme (Preston and Balepin 2002), the total pressure  $P_t = 113400$  Pa and total temperature  $T_t = 755$  K are assigned to the inlet boundary condition at the flight altitude of 26.82 km and Mach number of 3.5. For the high-speed flow, the scaled flow field of Stage-35 corresponding to the high-altitude state is obtained by the similarity criterion that maintains the same of inlet Mach number. The similarity criterion should keep the same coefficient of equivalent mass flow ( $\bar{G}$ ) between the similar flow field and the prototype flow field. The similarity criterion is given by:

$$\begin{aligned} (\bar{G}, \bar{N}) &= (G_0 \sqrt{T_{t0}} / P_{t0}, N_0 / \sqrt{T_{t0}}) \\ &= (G_1 \sqrt{T_{t1}} / P_{t1}, N_1 / \sqrt{T_{t1}}) \end{aligned} \quad (3)$$

where, the subscript of 1 and 2 denote the prototype and similar flow fields on the compressor inlet, respectively.

## 2.3 Numerical Calculation Accuracy

To verify the numerical procedure and methodology of simulation accuracy, a comparative result between numerical solution with SST  $\kappa-\omega$  turbulence model and NASA experimental data, as shown in Fig. 5. The numerical results for the total pressure ratio and efficiency of compressor are located between the design value and the

experimental value, and the trend of two characteristic lines are similar. Thus, it is believed that the numerical model used in this study agrees well with the experimental results. When the equivalent mass flow is about 0.00338, it is determined as the design value of compressor operation under the similarity flow field.

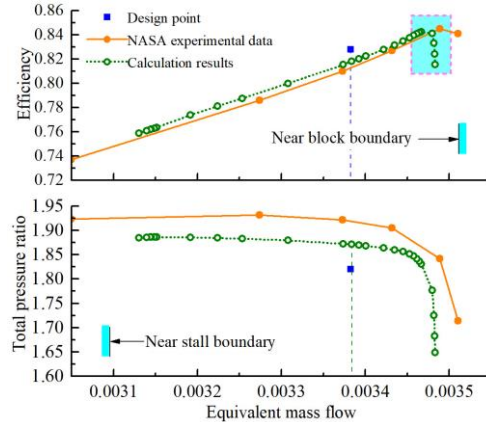


**Fig. 5. Comparisons of compressor characteristic between numerical and experimental results.**

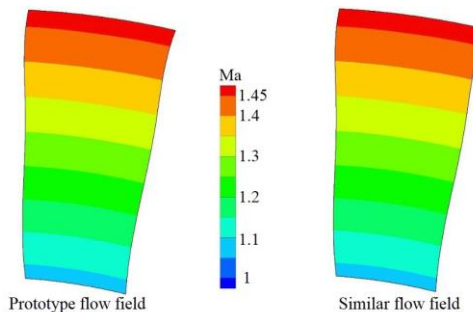


**Fig. 6. Comparisons of inlet Mach distributions between prototype and similarity flow field.**

In comparison with the prototype and similarity flow field as shown in Fig. 6, it can be seen that the Mach contours at each elementary section along the radial direction trend to approach the same. Furthermore, compared with the limiting streamline on the suction surface of rotor blade and the pressure surface of stator blade as shown in Fig. 7, it can be presented that the streamline distributions are also close to the same. The streamline separation regions both appear on the pressure surface of rotor blade for two flow fields because of the effect of the shock wave in the rotor passage, which conforms to the characteristics of transonic compressor. Then, it can be concluded that the application of similarity criterion is reliability for the present study.

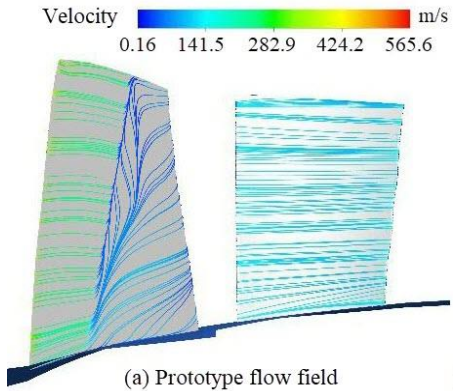
#### 2.4 Evaluation Indexes

Total pressure ratio in the pre-cooling section or compressor is defined as:

$$R_p = p_{t2} / p_{t1} \quad (4)$$

where,  $p_{t1}$  and  $p_{t2}$  are the mass-averaged total

pressure of the pre-cooling section or compressor at inlet and outlet, respectively.



(a) Prototype flow field

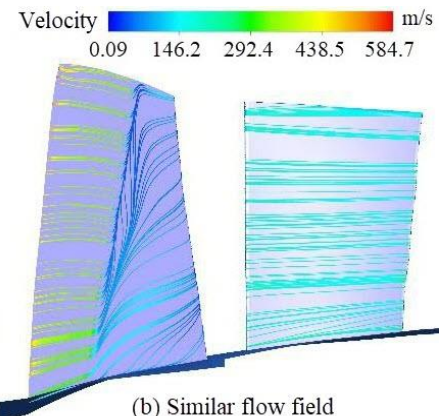


**Fig. 7. Comparisons of blade surface streamline between prototype and similarity flow field.**

The isentropic compression work of the compressor is obtained from the following equation:

$$W_{\text{isen}} = \frac{\kappa}{\kappa-1} R_g T_t \left( R_p^{\kappa/(\kappa-1)} - 1 \right) \quad (5)$$

where,  $R_g$  is the gas constant of 287 J/(kg·K),  $T_t$  is the total temperature at the compressor inlet,  $\kappa$  is the ratio of specific heat.

The actual consumption power of the compressor without the MIPCC method.

$$W_{\text{non-injection}} = L_{\text{tor, gas}} \cdot \omega \quad (6)$$

where,  $L_{\text{tor, gas}}$  is the torque induced by the gas acting on the rotor blade (*i.e.*, the gas source torque),  $\omega$  is angular velocity of the rotor.

The actual consumption power of the compressor with the MIPCC method.

$$W_{\text{injection}} = (L_{\text{tor, mix}} + L_{\text{tor, droplet}}) \cdot \omega \quad (7)$$

where,  $L_{\text{tor, mix}}$  is the torque induced by the mixed gas of water vapor and gas (*i.e.*, the mixed gas source torque),  $L_{\text{tor, droplet}}$  is the droplet source

torque given by

$$L_{\text{tor}, \text{droplet}} = \bar{p}Ar \quad (8)$$

where,  $\bar{p}$  the pressure of droplets acting on the rotor blade,  $A$  is the area on the rotor blade surface,  $r$  is the arm length which is equal to the radius of the rotor blade.

### 3. NUMERICAL RESULTS AND DISCUSSION

In the process of MIPCC in the pre-cooling section, the temperature of air will reduce due to the mass, momentum and energy exchange between the droplets and the surrounding airflow. Then, the remaining un-completely evaporated droplets and wet air mixture on the pre-cooling section outlet flow into the downstream compressor, which is of importance for the effect of compressor flow field. In order to analyze the changes and effects of MIPCC on the aerodynamic performance of the compressor, the flow field with and without the water injection rate of 2-8% and the droplet diameter of 10-20  $\mu\text{m}$  are compared and analyzed.

#### 3.1 Effect of Water Injection on Flow Field

Figure 8 shows the movement and temperature contour of droplets in the flow field with the water injection rate of 4% and the droplet diameter of 10  $\mu\text{m}$ . As depicted in the figure, the droplet temperature gradually increases along the streamwise and reaches a peak in the stator domain, indicating that the droplet absorbs the surrounding air temperature. Then, the temperature change of droplet in the flow field can reflect the strength of droplet evaporation. When the droplets move from 0 to 500  $\mu\text{s}$ , the ability of absorption of heat increases so that small droplet with higher temperature easily get the wet bulb temperature leading to its evaporation. However, when the droplets move to the front of compressor, the heat-absorbing ability of droplets decreases from 500 to 900  $\mu\text{s}$ . This phenomenon can substantiate that a small amount of non-evaporated droplets can continue to cool down the air temperature in the compressor. Actually, the MIPCC method can be understood as the wet compression or overspray (White et al. 2004 and Roumeliotis et al. 2007).

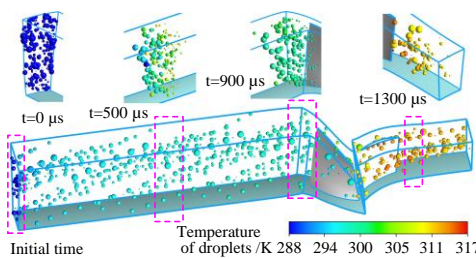
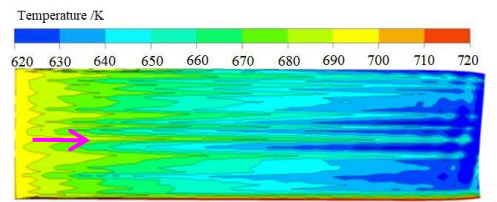


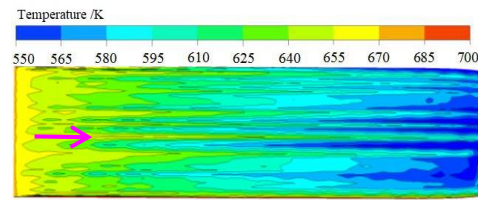
**Fig. 8. Temperature of droplets in the compressor coupled with the pre-cooling section.**

MIPCC in the pre-cooling section increases the instability for the flow field at high-speed air flow, as shown in Fig. 9 which is the static temperature

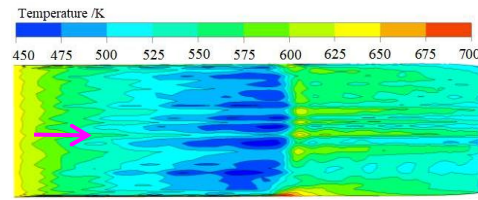
contour with the droplet size of 10  $\mu\text{m}$  and different water injection flow on the meridian surface of the pre-cooling section. It can be found that the temperature reduction in the pre-cooling section gradually increase as the water injection rate enhances from 2% to 8%. When the water injection rate is 2%, the temperature will decrease along the axial direction. The efficiency of evaporation for water droplets has a direct relationship with the temperature. When the airflow has just entered the pre-cooling section, the higher temperature has the larger temperature gradient in the pre-cooling section. At the water injection rate of 2%, the endothermic effect of water droplets greatly reduces the air temperature. In addition, the temperature reduces from 700 K at the inlet to 620 K at the outlet, representing an 11.4% reduction, which is less than that at water injection rate of 4% (i.e., 17.1%).



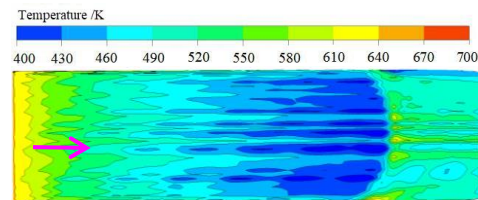
(a) water injection rate of 2%



(b) water injection rate of 4%



(c) water injection rate of 6%



(d) water injection rate of 8%

**Fig. 9. Static temperature contour at different water injection rates and the same droplet size of 10  $\mu\text{m}$  in the pre-cooling section.**

When the water injection rate increases to 6%, the velocity (Mach number) increases in the pre-cooling section due to the increase of inflow

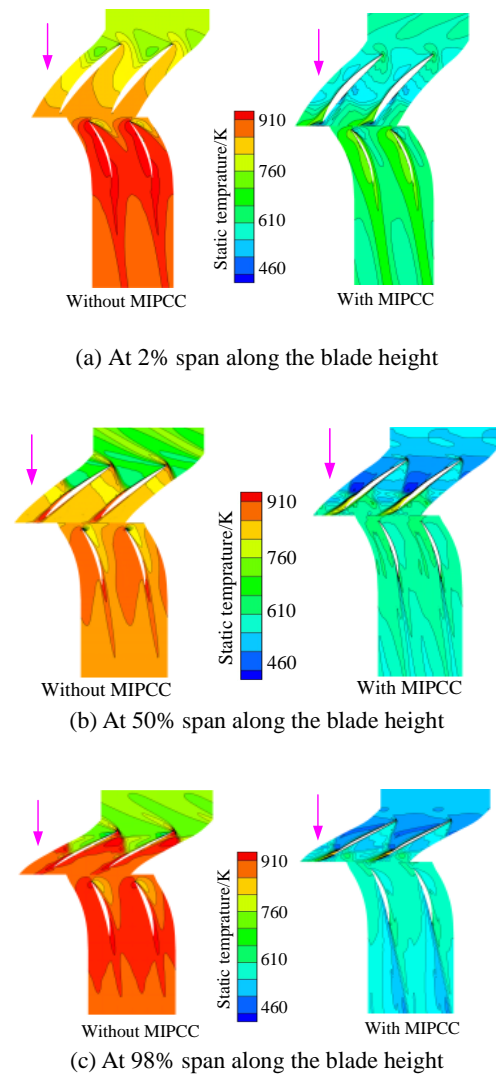
mass flow, and the shock wave is formed due to the disturbance of the coupling effect of water droplets and airflow. The temperature of airflow after the shock wave rises abruptly and the temperature gradient is greater than that at the inlet. Then, high temperature airflow continues to heat exchange with the water droplets, leading to a 150 K reduction at the outlet. When the water injection rate is 8%, the minimum temperature is about 400 K, and the shock wave and the local minimum temperature are shifted back; the temperature difference between inlet and outlet is about 200 K. Compared with Figs. 9 (a)-(b), it can be found that the temperature drop in the pre-cooling section is small when the water injection rate is small but the temperature at the compressor inlet is still high. Furthermore, the higher water injection rate is more likely to produce the shock wave to make more complicated for the flow field.

Figure 10 shows the temperature contours (4% water injection rate and 10  $\mu\text{m}$  mean droplet size) at different blade height with and without MIPCC. It can be seen from the figure that the temperature in the compressor without MIPCC increases with the streamwise; the higher temperature region mainly centers on the rotor and stator domains due to high speed rotation of rotor, high compression work and the convergent section of geometry structure. Simultaneously, the temperature along the radial direction presents uneven distribution where the temperature at 50% span is lower than that at 2% and 98% span locations. This phenomenon can be ascribed primarily to the inhomogeneous distribution for the upstream flow field since the droplets are easily to migrate radially under the centrifugal force of the rotor blade. In addition, since the secondary breakup of large droplet particle become small droplet particle, the smaller droplet particles will evaporate rapidly and completely, but the larger particle size will continue to absorb heat and evaporate. Clearly, the flow field temperature decreases after water injection. From the comparing results before and after water injection, it is the most important observation that, before water injection, a high temperature region exists after the streamline separation on the suction side of rotor blade and after the wake flow of blades. After water injection, however, these high temperature regions all decrease. It can be indicated that water injection in the pre-cooling section is of great importance for compressor flow field to further improve the compressor performance to a certain extent. Thus, the remaining un-completely evaporated droplets in the pre-cooling section can continue evaporation to conduct the mass and heat transfer in the compressor.

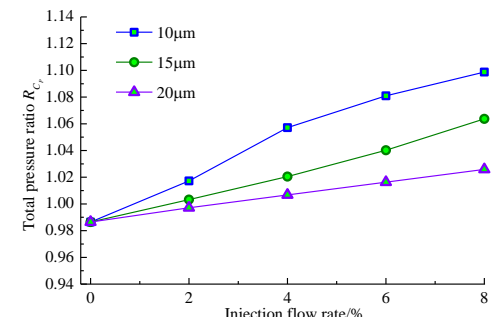
### 3.2 Influence of MIPCC on the Pre-cooling Section

Figure 11 shows the comparison of total pressure ratio in the pre-cooling section with and without the MIPCC technology. It can be seen from the figure, total pressure ratio of 0.986 in the pre-cooling section without MIPCC is caused by the total pressure loss leading to the reduction of total pressure on the pre-cooling section outlet less than

its inlet. With the increase of the water injection rate, the maximum total pressure recovery ability increases to 1.099 that is an increase of 11.5%. The smaller the droplet size of the injection flow, the greater the total pressure ratio. When the water injection rate is 8% and the droplet diameter is 10  $\mu\text{m}$ , the total pressure ratio of the pre-cooling section is 1.10, indicating that the smaller the droplet diameter is, the smaller the total pressure ratio is.



**Fig. 10. Static temperature contour at the water injection rate of 4% and droplet size of 10  $\mu\text{m}$ .**



**Fig. 11. Total pressure ratio in the pre-cooling**

### section at different water injection conditions.

The change of the velocity and the mass flow rate at the pre-cooling section inlet under different water injection conditions is shown in Fig. 12. Since the free stream velocity firstly flows into the air inlet, the mainstream on the pre-cooling section inlet is assumed that its velocity decrease to the subsonic range. The inlet axial velocity and mass flow of air after water injection are normalized with respect to  $v_0 = 270.114 \text{ m/s}$  and  $m_0 = 13.773 \text{ kg/s}$  before water injection. As shown in the figure, the inlet axial velocity increases significantly after water injection, then the mass flow of inflow air increases by 15.3-31.4%. And, the axial velocity and mass flow become greater at small droplet diameter. When the droplet diameter reaches to 10  $\mu\text{m}$ , the axial velocity and the mass flow rate of the flow field reach the peak value at the water injection rate of 6%, and the mass flow of inflow air is 31.4% higher than that without MIPCC. However, the velocity and mass flow have a downward trend when the water injection rate is increased to 8%. It can be concluded that the increase of the water injection rate in the appropriate range can significantly increase the flow mass of inflow air under high altitude and Mach number flight conditions.

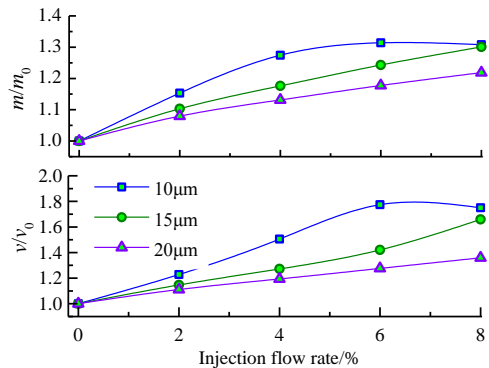


**Fig. 12. The change of axial velocity and mass flow of inflow air at the pre-cooling section inlet.**

The MIPCC technology can effectively reduce the inflow temperature, as shown in Fig. 13. The inlet static temperature in the pre-cooling section after water injection are normalized with respect to  $T_{s0} = 718.682 \text{ K}$  before water injection. With the increase of the water injection rate, the inflow temperature drops obviously, and the temperature reduction is in the range of 1.38-11.8%. When the droplet particles are small, the temperature drop is larger. However, when the particle size is 10  $\mu\text{m}$  and the water injection rate is 6%, the inflow temperature no longer increases with the increase of water injection rate.

### 3.3 Influence of MIPCC on the Compressor

From the above analysis, it can be seen that the increase of the water injection rate could not continuously increase the temperature drop in the pre-cooling section, but it can continuously reduce the outlet temperature in the pre-cooling section, that is, the inlet temperature in the compressor. Figure 14 shows the static temperature at

compressor inlet and total temperature ratio of compressor under different MIPCC conditions. The inlet static temperature in the compressor after water injection are normalized with respect to  $T_{02} = 718.457 \text{ K}$  before water injection. Due to the viscous effect on the non-free slip wall, the inlet temperature of compressor with the injected water droplets is slightly higher than that of the pre-cooling section. After water injection, the effect of the droplets on the absorption heat of airflow during the evaporation phase change becomes conspicuous, and the airflow temperature at compressor inlet is reduced. This temperature at the compressor inlet reaches a heat load of 700 K at the water injection rate of 2%, while the 8% water injection rate drops to about 500 K which is 20.4% lower than that at the inlet of pre-cooling section. From the static temperature contour in Fig. 10, the un-completely evaporated droplets in the pre-cooling section flow into the compressor to heat absorption in the wet compression process. Then, the temperature ratio of compressor continues to decrease by 3.6-16.14% as water injection rate increases. In the water injection rate of 6-8%, the temperature ratio begins to change in the steady state, indicating that the change ranges of temperature ratio are small due to the smaller the droplet particles.

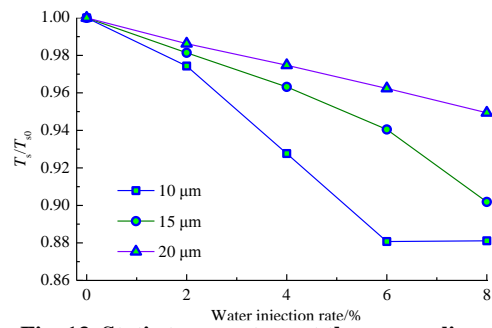


**Fig. 13. Static temperature at the pre-cooling section inlet for different MIPCC conditions.**

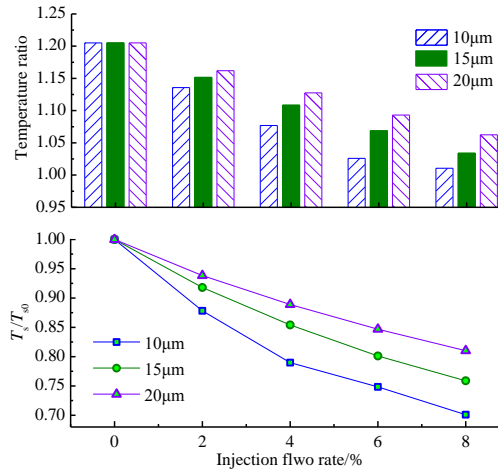


**Fig. 14. Change of temperature ratio and inlet temperature at different MIPCC conditions.**

Figure 15 exhibits the total pressure ratio of the

compressor under different MIPCC conditions. As it is shown, the compressor pressure ratio is around 1.87 without water injection. When water injection is in the range of 0-8%, there is compression pressure ratio increase but then the total pressure ratio decreases slightly to an extent. And later as injected mass flow rate significantly increases, total pressure ratio of compressor decreases. The total pressure ratio reaches the peak value at which the total pressure ratio is increased by 0.91% compared without water injection, indicating that the increase of the water injection rate is not conducive to the increase of the total pressure ratio of the compressor. When the droplet particle size is in the range of 10-20  $\mu\text{m}$ , the total pressure ratio is proportional to the particle size, and the effect of increasing the total pressure ratio is more obvious in the case of the larger water injection rates and droplet sizes. It can be indicated that the larger droplet particles will make more smaller droplets with incomplete evaporation in the pre-cooling section and then flows into the compressor. When the droplet diameter is 10  $\mu\text{m}$  and the water injection rate is 8%, the total pressure ratio of compressor is reduced by about 0.09%.

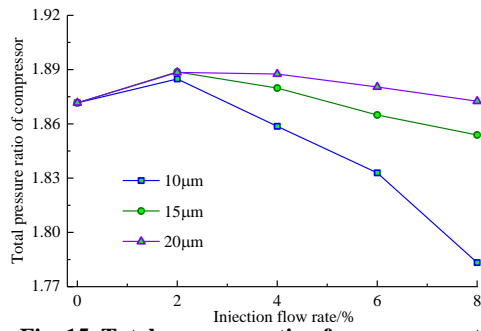


Fig. 15. Total pressure ratio of compressor at different MIPCC conditions.

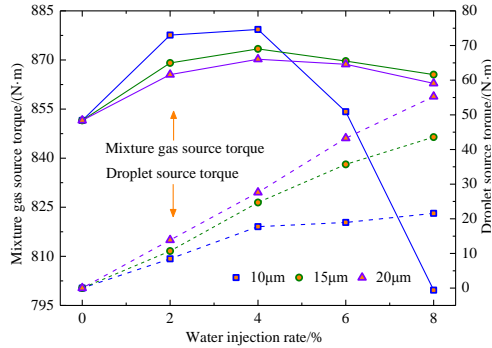


Fig. 16. Variation of the rotor blade torque induced by the wet air mixture and droplets.

The variation of the torque induced by wet air mixture and droplets is shown in Fig. 16. When the water injection rate is 2-4%, the mixed gas source torque is increasing and up to the local maximum value of 879.313 N·m where the water injection rate is 4% with the droplet diameter of 10  $\mu\text{m}$ , which increases by 3.3% compared without the MIPCC. When the water injection rate is 4-8%, the mixture gas source torque shows a decreasing trend, and for the droplet particles of 10  $\mu\text{m}$ , the mixture gas

source torque changes steeply in the decreasing range and is lower than the torque value corresponding to non-injection flow. However, part of the torque of the compressor is caused by the mixture gas source torque, and the other part is induced by the droplets.

From the change of the droplet source torque in Fig. 16, it can be seen that, with the increase of the water injection rate, the airflow carrying droplet particles increase in the compressor, and the action of the rotor blade causes the increase of the extra torque. Since the ability following with the flow for the larger droplets are weaker than the smaller droplets, the droplets with the small particles are more likely to escape from the trajectories of the main flow and impinge on the pressure surface of rotor blade. The additional torque produced by the larger droplet size is much more than the smaller droplet size at the same of the water injection rate. Moreover, the torque caused by the droplet reaches the local maximum of 55.28 N·m at the water injection rate of 8% and droplet size of 20  $\mu\text{m}$ .

The actual compression consumption work is different from the specific compression consumption work in the compressor under different MIPCC conditions. Figure 17 shows the change of the actual and isentropic comparison consumption work. The specific compression work after water injection is normalized with respect to the actual specific compression work  $w_0 = 180.14 \text{ kJ/kg}$  before water injection. As depicted in the figure, it can be seen that, although the actual compression consumption work of compressor increases in a certain range after water injection, the actual and isentropic comparison consumption work decrease. This phenomenon is because the total pressure ratio and specific heat capacity at constant pressure increase in the pre-cooling section after water injection so that the compressor inlet temperature significantly reduces by comparison with the dry air condition. Moreover, it can be concluded that the temperature at the compressor inlet is low at the larger water injection rate and smaller droplet diameter, resulting in what the actual and isentropic comparison consumption work with the MIPCC are less than that without the MIPCC. In the droplet particle size of 10  $\mu\text{m}$  and water injection rate of 8%, its actual compression consumption work is decreased to 0.72 relative to without water injection.

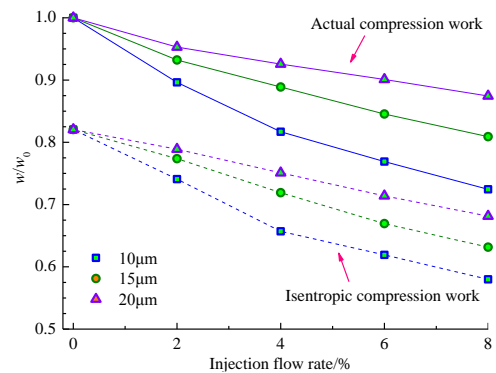
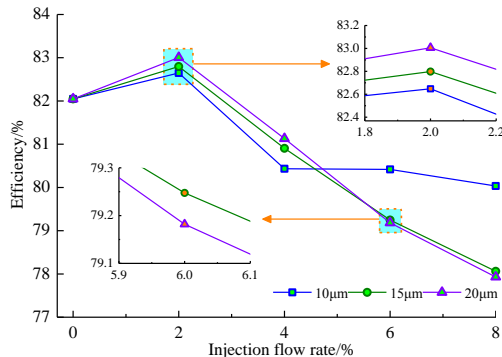


Fig. 17. The actual and isentropic specific compression consumption work of compressor.



**Fig. 18. Total-total isentropic compression efficiency at different MIPCC conditions.**

Figure 18 shows the total-total isentropic compression efficiency of the compressor under different water injection conditions. In the range of 0-8% for the water injection rate, the efficiency shows a monotonous "increasing to decreasing" change and reaches a maximum value at the water injection rate of 2% where the efficiency increases by 1.2% higher than that without water injection. When the water injection rate is less than or equal to 4%, the smaller droplet size has a lower efficiency. However, the smaller droplet diameter has higher efficiency when the water injection rate is more than 4%. Then, the efficiency is reduced to the local minimum when the water injection rate is 8%, and the efficiency is reduced by 2.5% compared without water injection at the droplet size of 10  $\mu\text{m}$ .

#### 4. CONCLUSION

In this study, the water injection in front of aero-engine compressor at the high-altitude 3.5 Mach number flight is investigated, and the influence of water injection conditions on the aerodynamic performance of compressor is analyzed. The main conclusions can be drawn as follows.

With the increase of water injection rate, the inflow velocity enhances, and then the evaporation rate of droplets reduces so that more droplets enter the compressor. For the larger water injection rate, the shock wave is easy to produce in the pre-cooling section; the shock wave appears near the trailing edge of the pressure surface for the rotor blade, which increases the radial migration of the airflow.

In the range of 0-8% water injection rates and 10-20  $\mu\text{m}$  droplet diameters, total temperature ratio of compressor reduces by 3.6-16.14%, the mass flow rate of the incoming flow increases by 15.3-31.4%; total pressure ratio of compressor increases by 0.91%. Moreover, total pressure ratio and compression consumption work increase at large droplet diameter.

With the increase of water injection rate, the specific compression work decreases gradually, and the efficiency shows a trend of "increasing-to-decreasing". At the water injection rate of 2%, the compressor efficiency increases 1.2% higher than that before water injection.

#### ACKNOWLEDGEMENTS

The authors would like to thank the support of the National Natural Science Foundation of China (No. 517741901) and the Fundamental Research Funds for the Central Universities (No. HEUCF180305). In addition, Aqiang Lin especially wishes to thank the care and love from his mom Xiuyu Wu.

#### REFERENCES

- Balepin, V. and G. Liston (2001). The steamjet: Mach 6+ turbine engine with inlet air conditioning. In *Proceedings of 37th AIAA/ASME/SAE/ASEE Joint Propulsion Conference and Exhibit*, Salt Lake, Utah, AIAA-2011-3238.
- Balepin, V., C. Bruno and A. Ingenito (2003). Evaluation of the combustion process in the mass injection precompression cooling engine. In *Proceedings of XVI International Symposium on Air Breathing Engines*, ISABE-2003-1127.
- Bayraktar, S. and T. Yilmaz (2016). Dominant Vortex Structures in Transverse Jets. *Journal of Applied Fluid Mechanics* 9(5), 2403-2411.
- Carter, P., V. Balepin, T. Spath and C. Ossello (2003). MIPCC technology development. In *Proceedings of 12th AIAA International Space Planes and Hypersonic Systems and Technologies*, Norfolk, Virginia, AIAA-2003-6929.
- David, A. Y. and R. O. John (2005). Responsive access small cargo affordable launch (RASCAL) independent performance evaluation. In *Proceedings of AIAA/CIRA 13th International Space Planes and Hypersonics Systems and Technologies*, AIAA-2005-3241.
- Jiang, F., H. Wang, Y. Wang and J. Xiang (2016). Simulation of flow and heat transfer of mist/air impinging jet on grinding work-piece. *Journal of Applied Fluid Mechanics* 9(3), 1339-1348.
- Kim, K. H. and H. Perez-blanco (2006). An assessment of high-fogging potential for enhanced compressor performance. In *Proceedings of ASME Turbo Expo 2006: Power for Land, Sea, and Air*, Barcelona, Spain, 693-701.
- Lin A. Q., Y. G. Sun, H. Zhang, X. Lin, L. Yang and Q. Zheng (2018). Fluctuating characteristics of air-mist mixture flow with conjugate wall-film motion in a compressor of gas turbine. *Applied Thermal Engineering* 142, 779-792.
- Ma, H. (2013). *Performance Investigation on Anticer of Composite Engine Inlet Vane*. Ph. D. thesis, the Nanjing University of Aeronautics and Astronautics, Nanjing, China.
- Mehta, U., J. Bowles and J. Melton (2015). Water injection pre-compressor cooling assist space access. *Aeronautical Journal* 119, 145-171.

- Miyagi, H., H. Miyagawa, T. Monji, K. Kishi, T. Powell and M. Morita (1995). Combined cycle engine research in Japanese HYPR project. In *Proceedings of 31st AIAA/ASME/SAE/ASEE Joint Propulsion Conference and Exhibit*, San Diego, CA, AIAA-95-2751.
- Neupert, N., B. Ober and F. Joos (2014). Experimental investigation on droplet behavior in a transonic compressor cascade. *Journal of turbomachinery* 137(3), 031009.
- Preston, H. C. and V. Balepin (2002). Mass injection and pre-compressor cooling engines analyses. In *Proceedings of 38th AIAA/ASME/SAE/ASEE Joint Propulsion Conference and Exhibit*, Indianapolis, Indiana, AIAA-2002-4127.
- Reid, L. and R. D. Moore (1978). Design and overall performance of four highly-loaded, high-speed inlet stages for an advanced, high-pressure-ratio core compressor. NASA Technical Report 1337.
- Roumeliotis, I. and K. Mathioudakis (2007). Water injection effects on compressor stage operation. *ASME Journal of Engineering for Gas Turbines and Power* 129, 778-798.
- Rui, C. S., C. Zhang and D. F. Yue (2015). Technical study and development of mass injection pre-compressor cooling turbine engine. *Aeronautical Science and Technology* 26, 53-59.
- Sanaye, S. and M. Tahani (2010). Analysis of gas turbine operating parameters with inlet fogging and wet compression processes. *Applied Thermal Engineering* 30(2), 234-244.
- Steelant, J. (2011). Sustained hypersonic flight in Europe: first technology achievements within LAPCAT II, In *Proceedings of 16th AIAA/DLR/DGLR International Space Planes and Hypersonic Systems and Technologies Conference*, AIAA-2011-2243.
- Sun, L. X., Q. Zheng, Y. J. Li and R. K. Bhargava (2012). Numerical simulation of a complete gas turbine engine with wet compression. *Journal of engineering for gas turbines and power* 135(1): 012002.
- Tanatsugu, N., T. Sato and V. Balepin (1997). Development study on ATREX engine. *Acta Astronautica* 41(2-8), 851-862.
- Vladimir, B. (2007). High speed propulsion cycles, RTO-AVT-VKI LS CSP-07-5052. Rhode Saint Genese: VKI.
- Wang, Y. and Z. G. Wang (2016). Review on precooled combined cycle engine and mini- and micro-channel flow heat transfer. *Journal of Astronautics* 37(1), 11-20.
- White, A. J. and A. J. Meacock (2004). An evaluation of the effects of water injection on compressor performance. *Transactions of the ASME Journal of Engineering for Gas Turbines and Power* 126(4), 748-754.
- White, A. J. and A. J. Meacock (2010). Wet compression analysis including velocity slip effects. In *Proceedings of ASME Turbo Expo 2010: Power for Land, Sea, and Air*, Glasgow, UK, 953-963.
- Zou, Z. P., H. X. Liu, H. L. Tang, M. Wan and H. W. Wang (2015). Study on precooling technology of hypersonic aeroengine. *Acta Aeronautica Et Astronautica Sinica* 36(8), 2544-2562.